Volume 55
Number 10
10 March 2026
Pages 4003-4344

Dalton Transactions

An international journal of inorganic chemistry

rsc.li/dalton

ISSN 1477-9226

ROYAL SOCIETY OF CHEMISTRY

COMMUNICATION

Anjana Devi *et al.*

Ruthenium(II) carbonyl amidates – a new class of precursors for atomic layer deposition

Dalton Transactions

ROYAL SOCIETY OF CHEMISTRY

COMMUNICATION

View Article Online
View Journal | View Issue

Cite this: *Dalton Trans.*, 2026, **55**, 4046

Received 30th October 2025,
Accepted 11th January 2026

DOI: 10.1039/d5dt02610e

rsc.li/dalton

Ruthenium(II) carbonyl amidates – a new class of precursors for atomic layer deposition

Jorit Obenlüneschloß, [a] Cara-Lena Nies, [b] Michael Gock,[c] Michael Unkrig-Bau,[c] Jan-Niklas Huster, [a] Michael Nolan [b] and Anjana Devi *[a,d,e]

Ru-based thin films are essential for electronics and catalysis. Their growth through atomic layer deposition (ALD) depends on precursors that balance reactivity, volatility, and thermal stability. We present the first Ru dicarbonyl bisamidate complexes as a new and promising class of ALD precursors for Ru-based materials. Modifying the substitution pattern of the amidate ligands yielded $[Ru(CO)_2(N\text{-}sBuiPrAD)_2]$, as a volatile liquid precursor with excellent thermal properties. First principles simulations predict favorable interactions with common ALD co-reactants, indicating its potential for thin film deposition.

Applications of ruthenium in catalysis and nanoelectronics are increasing the demand for small Ru complexes. Ru promotes heterogeneous catalysis in Fischer–Tropsch syntheses,[1,2] methanation,[3,4] and the alkaline hydrogen evolution reaction (HER).[5] Ru complexes are equally attractive in homogeneous catalysis, such as the Grubbs catalyst,[6–8] in cross-coupling,[9,10] and in dehydrogenation reactions.[11,12] Ru is the leading candidate to replace Cu as the interconnect metal in the lowest metallization levels of integrated circuits.[13] Its resistivity is less thickness-dependent than that of Cu, and Ru can be introduced without liner or diffusion barrier layers.[14,15] A resistance reduction of up to 60% is expected when Ru vias are implemented with Cu wires.[16]

Next to Ru, RuO_2 is also an intriguing material that exhibits high conductivity, making it relevant for future electrodes in dynamic random access memory (DRAM) and as an interlayer between Ru electrodes and dielectric materials.[17,18] Its conductivity and high specific capacitance enable RuO_2 to be prominently used in energy conversion and storage.[19,20] An important application of RuO_2 is as catalyst for the oxygen evolution reaction (OER).[21,22] Recently, RuO_2 has gained significant interest as a prototypical altermagnetic material.[23,24]

To deposit Ru, RuO_2, or any Ru-containing thin film on challenging dimensions and geometries of integrated circuits or high-surface-area substrates for catalysis, chemical vapor deposition (CVD) and atomic layer deposition (ALD) are the most preferred thin film deposition techniques. Both methods require precursors that possess suitable physicochemical properties. For industrial use in high-volume manufacturing (HVM), liquid precursors are preferred due to their reliable evaporation and ease of handling. Current Ru precursor candidates do not fully meet the required criteria in terms of volatility and reactivity. There are intensive research efforts to develop superior Ru precursors.[25] Notable examples of recent precursor developments include: TRuST (highly volatile; ALD of Ru and RuO_2 with O_2),[26,27] T-Rudic (dinuclear; ALD of Ru with H_2O or O_2),[28] $Ru(DMBD)(CO)_3$ (0-oxidation state; ALD of Ru and RuO_2 with O_2),[29] Ru carbonyl acetamidinate (*N*,*N*′-chelating; ALD of Ru with NH_3 and O_2),[30,31] and HeRu31 (Ru-alkyl).[32]

Here, we introduce a new ligand to Ru and report, for the first time, Ru dicarbonyl bisamidate complexes, proposing them as ALD precursors. When an amide is used as an amidate ligand, it can adopt a beneficial 1,3-conjugated chelating bonding motif with N and O binding sites, stabilizing and shielding the metal center.[33] However, it can also display bridging coordination or be monodentately bound by either the nitrogen or oxygen atom.[34] The binding modes depend on steric factors, which determine denticity, and electronic factors such as the molecular charge distribution that influence the possible interactions of the binding atom with the metal center.[35] Similar to amidinates, *e.g.* the structurally similar Ru carbonyl acetamidinate reported by Li *et al.*,[36] amidate substitution patterns can vary based on the side chain bound to the nitrogen and the backbone substituent. However, amidates have only one such side chain because of the divalent binding oxygen atom replacing the trivalent nitrogen.

[a]*Inorganic Materials Chemistry, Ruhr University Bochum, Bochum, 44801 Germany. E-mail: a.devi@ifw-dresden.de*
[b]*Tyndall National Institute, Lee Maltings, University College Cork, Cork T12 R5CP, Ireland*
[c]*Heraeus Precious Metals GmbH & Co. KG, 63450 Hanau, Germany*
[d]*Leibniz Institute for Solid State and Materials Research, IFW Dresden, 01069 Dresden, Germany*
[e]*Chair of Materials Chemistry, TU Dresden, 01069 Dresden, Germany*

With one fewer sidechain, the molecular mass is significantly lower than that of an otherwise identically substituted amidinate. This reduction is expected to improve amidate evaporation relative to acetamidinates. Furthermore, the asymmetry created by the single side chain will likely enhance volatility. Substituting nitrogen with oxygen while maintaining the delocalized coordination motif should also improve the stability of amidate complexes through robust Ru–O interactions. Further, the unique mixed Ru–O and Ru–N coordination can enable new deposition pathways that are not accessible with primarily C-coordinated Ru precursors, which often exhibit significant nucleation delays on SiO_2.[37–39]

Unlike amidinate (transition-)metal complexes, amidate complexes are not widely used for ALD or CVD, except for uranium(IV) and zirconium(IV) amidates, which are utilized for CVD of UO_2 and ZrO_2, respectively.[40,41] This may be attributed to the sub-optimal thermal properties of many amidate compounds, necessitating aerosol-assisted CVD (AACVD) in the case of Zr. In the case of U, insufficient thermal stability is evidenced by the high residual masses observed in thermogravimetric analysis (TGA). Further examples of amidate ligands are compounds explored as potential single-source precursors for ThO_2.[42] For these amidate precursors (U, Zr, Th), an alkene elimination pathway, evidenced by NMR studies, was described, yielding the respective oxides.[40–42] Additionally, many amidate complexes are reported in the patent literature, including heteroleptic Ti and Zr amidate amides, as well as an ALD process using O_3 for TiO_2.[43] Given these promising but limited examples of amidate-based precursors, we explored amidates in small Ru complexes, evaluated how different substitution patterns influence their properties, and predicted their interactions with ALD-relevant co-reactants.

Ru carbonyl amidate complexes were synthesized *via* a salt metathesis route from tricarbonyldichlororuthenium(II) dimer and *in situ* lithiated acyl amides, as depicted in Fig. 1a. An extended discussion of the synthesis is provided in the SI. Both (**1**) [Ru(CO)$_2$(N-iPr*t*BuAD)$_2$] and the switched substitution pattern (**2**) [Ru(CO)$_2$(N-*t*BuiPrAD)$_2$] were isolated as clear to pale yellow solids in low yields (around 10%). In contrast, (**3**) [Ru(CO)$_2$(N-*s*BuiPrAD)$_2$], the *sec*-butyl substituted variant, was isolated as a yellow oil with a high yield of 82% (inset Fig. 1e).

The purity of the complexes was assessed by ^{1}H and ^{13}C NMR, elemental analysis, and FTIR (Fig. S2 and S3, SI). For (**1**) and (**2**), the isopropyl methyl groups are magnetically inequivalent, regardless of whether the isopropyl group is bound to the nitrogen atom or to the backbone, resulting in two doublets in the ^{1}H NMR. Compound (**3**) shows even more complicated spectra. Not only did the coupling of the *sec*-butyl group add complexity, but the side chains on both ligands are magnetically non-equivalent, resulting in double signals for the chemically identical groups. Additionally, the inversion center of the *sec*-butyl group means that (**3**) consists of diastereomers, with the methylated carbons within the *sec*-butyl groups acting as chiral centers. This is evident in the NMR spectra, as shown by the significant degree of overlap and splitting in the ^{1}H NMR as well as the appearance of double signals in the ^{13}C NMR.[44]

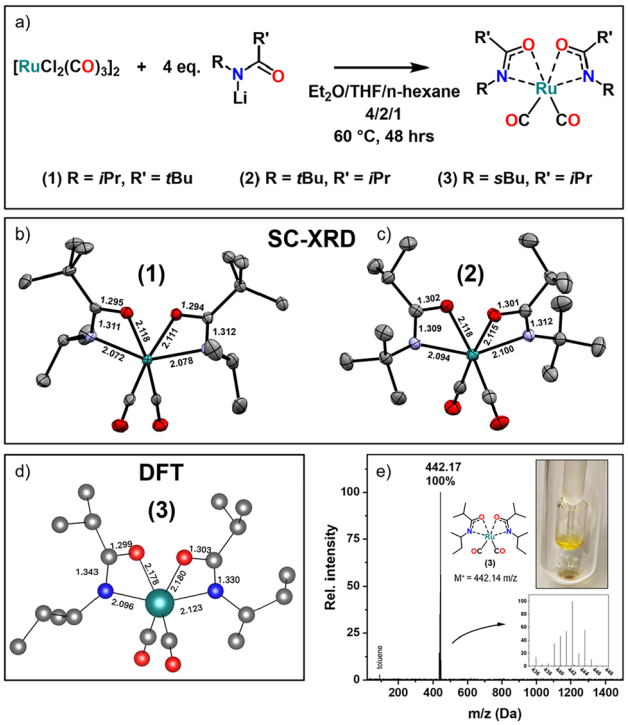

Fig. 1 (a) Synthesis scheme for compounds (**1**), (**2**), and (**3**). Molecular crystal structure of (b) (**1**) and (c) (**2**). Thermal ellipsoids are shown with 50% probability. (d) DFT structure of (**3**). Hydrogen atoms are omitted for clarity. Notable bond lengths are given in Å. (e) LIFDI-MS spectrum for (**3**), with the inset graph showing the mass distribution of the molecular ion peak, the inset picture displays the freshly distilled yellow compound (**3**) in a distillation basket.

Solid state structures of (**1**) and (**2**) were determined from single crystal X-ray diffraction (SC-XRD) experiments, see Fig. 1b and c and Table S4 for additional crystallographic details. (**1**) crystallizes in space group $P\bar{1}$ (no. 2) in the triclinic system, while (**2**) crystallizes in the $P2_1/c$ space group in the monoclinic system. Each has one mononuclear Ru complex as the asymmetric unit. Both complexes exhibit a distorted octahedral coordination geometry with a *cis* ligand arrangement where the carbonyl ligands are adjacent to each other. The molecular structure closely resembles the related acetamidinate complexes.[36] Despite the lower degree of steric shielding of the metal center, compared to the acetamidinates, due to only one side chain per amidate ligand in proximity to the metal center, the Ru(II) carbonyl amidate complexes are exclusively mononuclear. In contrast, Neumann *et al.* reported that for Ru(0), dimeric and even polymeric amidate Ru(0) solvent adducts were formed, connected by protonated amidates.[45] In the solid state structures, the Ru–N and Ru–O bond distances differ slightly, with average Ru–N bond distances of 2.075 Å and 2.097 Å and Ru–O bond distances of 2.115 Å and 2.150 Å for (**1**) and (**2**), respectively. The Ru–N bond carries the highest degree of covalent character, whereas the Ru–O bond displays weaker bonding, as indicated by its longer distance, and likely exhibits a more coordinative nature. Further, the N–C and C–O

distances are asymmetric; the formally C═O double bond is noticeably longer, with a C–O distance of 1.30 Å in comparison to C═O double bonds in amides with bond distances of 1.25 Å.[46] This elongation is an effect of the electron delocalization occurring in the 4-membered ring formed by the 1,3-chelating ligand and the metal center.

To elucidate the structure of (**3**), we used density functional theory (DFT). The calculated structure and the configuration with the carbonyls in *cis*-configuration and the 1,3-N,O bridging coordination of the amidate ligands were almost identical to the structures of (**1**) and (**2**) (Fig. 1d). The calculated bond lengths of (**3**) were also very close to those obtained from the single crystal structures. The DFT-derived molecular structures of (**1**) and (**2**) are discussed in the SI.

Liquid-injection field desorption ionization mass spectrometry (LIFDI-MS) is particularly suited to characterize precursors, because it does not require harsh ionization conditions and facilitates the detection of the molecular ion peak more easily.[47] As shown in Fig. 1e, the molecular ion peak of (**3**) was detected with 100% relative intensity, supporting its expected and calculated mononuclear nature. Similarly, the molecular ion peaks of (**1**) and (**2**) were detected as the only *m*/*z* signal in their respective LIFDI-MS spectra aside from the solvent (Fig. S5, SI). This indicates the high purity achieved through sublimation and distillation for all compounds.

The stability of (**3**) in ambient conditions was confirmed by FTIR spectroscopy, highlighting its ease of handling (Fig. S4, SI).

To assess the suitability of the Ru carbonyl amidate complexes as ALD precursors, their volatility and thermal stability were examined by TGA. As shown in Fig. 2a, all three complexes exhibit a distinct one-step mass loss event with step temperatures around 170 °C. Table S5 in the SI summarizes all thermal data. Compound (**2**) evaporates cleanly, while complexes (**1**) and (**3**), which contain a proton in the β-position to the metal, exhibit slightly higher residual masses. Although all three may be susceptible to an alkene elimination decomposition pathway similar to that observed for U, Zr, and Th precursors, this is unlikely within the TGA temperature range before evaporation; instead, a minor degree of β-hydride elimination is postulated for (**1**) and (**3**).[40–42] The residual masses observed for (**1**) and (**3**) cannot be assigned to any byproduct formed (theoretically expected to be 22.9% for Ru and 30.1% for RuO_2), as there is a coupling between evaporation and decomposition in the temperature range (150 °C and 225 °C) which distorts the analysis of the residual masses. To accurately determine their volatility, vapor pressures were estimated using the Langmuir and Clausius–Clapeyron equations, as shown in Fig. 2b.[48,49] The temperature at which 1 Torr of vapor pressure is reached ($T_{1\ \mathrm{Torr}}$) indicates that (**3**) is the most volatile, with a $T_{1\ \mathrm{Torr}}$ of 103.1 °C. The liquid aggregation state of (**3**) is advantageous for an ALD precursor because it does not succumb to particles aggregating or sintering, which can impede constant evaporation. Simultaneous differential scanning calorimetry (DSC) and TGA measurements revealed the melting points of (**1**) and (**2**) as 74 °C and 104 °C, respectively (Fig. S9, SI), compared to 211 °C for the Ru carbonyl acetamidinate.[36] This illustrates how different substitution patterns and ligand structure significantly influence aggregation, melting behavior, and volatility. Although all three compounds have the same molecular weight, varying the alkyl side chains, affects their volatility. This is evident from their vapor pressures; introducing the asymmetric *sec*-butyl side chain reduces the $T_{1\ \mathrm{Torr}}$ by nearly 20 °C. Amidate ligands notably improve volatility compared to the related Ru carbonyl acetamidinate, which features a step temperature of 220 °C (Fig. S10, SI). The lighter amidate ligand enhances volatility, with (**1**), (**2**), and (**3**) having only about 90% of the mass of the Ru carbonyl acetamidinate. This places the Ru amidates at the higher-volatility end of the Ru precursor range, with many precursors exhibiting primary mass-loss events between 200 °C and 250 °C.[50–53] According to the literature, the authors are aware of only two Ru(0) examples with higher volatility: TRuST and Ru(DMBD)$(CO)_3$.[26,29]

An initial assessment of the reactivity of (**3**) toward ALD co-reactants was performed using DFT, which has previously been used to quickly evaluate precursor reactivity without complex ALD surface chemistry simulations, to calculate interaction energies with common ALD co-reactants.[54–56] (**3**) interacts exothermically with NH_3, O_2, and O radicals, which could be beneficial for Ru and RuO_2 ALD (Fig. 3). The most exothermic interaction energy of −1.35 eV is observed for the O radical. Reactions to form CO_2 are most favorable, indicating that the carbonyl ligand will be eliminated first. Mildly exothermic interactions with H_2O were also computed. A complete set of interaction energies with co-reactants is provided in Table S1 in the SI, along with a detailed discussion of DFT-derived structures, reactivities, and

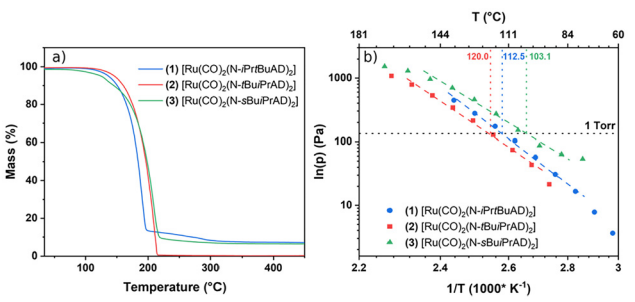

Fig. 2 (a) TGA of compounds (**1**), (**2**), and (**3**). (b) Clausius–Clapeyron plot showcasing the temperature vapor pressure relationship of the investigated compounds.

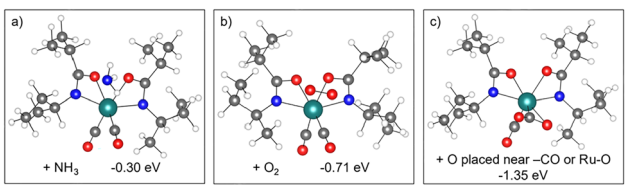

Fig. 3 Structures and interaction energies of (**3**) with potential co-reactants, (a) NH_3, (b) O_2, and (c) O radicals. Colours: H = white, C = grey, N = blue, O = red, Ru = green.

probable reaction products for (**1**) and (**2**), which are largely similar to (**3**) except for the endothermic formation of a Ru–O bond when (**1**) interacts with an O radical.

In summary, we successfully synthesized ruthenium dicarbonyl bisamidate complexes as a new class of small, volatile Ru ALD precursor compounds. The strategic use of amidate ligands results in a liquid at room temperature for $[Ru(CO)_2(N\text{-}s\text{BuiPrAD})_2]$ (**3**). SC-XRD, LIFDI-MS, and DFT confirm a monomeric molecular structure and high purity. TGA demonstrates the necessary high volatility and thermal stability for ALD processing. Compound (**3**) exhibits the highest volatility and lowest $T_{1\ \mathrm{Torr}}$ of 103 °C, which is a significant improvement over the structurally related Ru carbonyl acetamidinate. Favorable interaction energies of (**3**) with NH_3, O_2, and O radicals indicate its potential as an ALD precursor for Ru or RuO_2. This work not only reports the synthesis of new Ru complexes but also paves the way for further exploration and optimization of amidate ligands in ALD processing to advance Ru deposition technologies.

Conflicts of interest

There are no conflicts to declare.

Data availability

The data supporting this article are included in the supplementary information (SI). Supplementary information is available. See DOI: https://doi.org/10.1039/d5dt02610e.

CCDC 2487934 (**1**) and CCDC 2487935 (**2**) contain the supplementary crystallographic data for this paper.[57a,b]

Acknowledgements

This work was funded by Heraeus Precious Metals GmbH & Co. KG. AD acknowledges the Leibniz Association (ASPIRE-2D project-155/2023) and the Fraunhofer Society (Attract project-40-00643) for supporting this work.

References

1 V. Ragaini, R. Carli, C. L. Bianchi, D. Lorenzetti, G. Predieri and P. Moggi, *Appl. Catal., A*, 1996, **139**, 31–42.
2 W.-Z. Li, J.-X. Liu, J. Gu, W. Zhou, S.-Y. Yao, R. Si, Y. Guo, H.-Y. Su, C.-H. Yan, W.-X. Li, Y.-W. Zhang and D. Ma, *J. Am. Chem. Soc.*, 2017, **139**, 2267–2276.
3 C. Shen, M. Liu, S. He, H. Zhao and C. Liu, *Chin. J. Catal.*, 2024, **63**, 1–15.
4 C. Yang, T. Zhang, Y. Chen, W. Wang, H. Zhuo, X. Yang and Y. Huang, *ACS Catal.*, 2023, **13**, 11556–11565.
5 B.-L. Lin, X. Chen, B.-T. Niu, Y.-T. Lin, Y.-X. Chen and X.-M. Lin, *Catalysts*, 2024, **14**, 671.
6 J. Louie and R. H. Grubbs, *Organometallics*, 2002, **21**, 2153–2164.
7 G. C. Vougioukalakis and R. H. Grubbs, *Chem. Rev.*, 2010, **110**, 1746–1787.
8 T. Bano, A. F. Zahoor, N. Rasool, M. Irfan and A. Mansha, *J. Iran. Chem. Soc.*, 2022, **19**, 2131–2170.
9 J.-X. Xu, F. Zhao, R. Franke and X.-F. Wu, *Catal. Commun.*, 2020, **140**, 106009.
10 Y. Na, S. Park, S. B. Han, H. Han, S. Ko and S. Chang, *J. Am. Chem. Soc.*, 2004, **126**, 250–258.
11 P. Devi, M. Kannan, Kiran, Virender, A. Kumar and S. Muthaiah, *J. Organomet. Chem.*, 2022, **980–981**, 122515.
12 R. E. Rodríguez-Lugo, M. A. Chacón-Terán, R. Wolf and V. R. Landaeta, *Inorg. Chim. Acta*, 2024, **573**, 122314.
13 L. G. Wen, P. Roussel, O. V. Pedreira, B. Briggs, B. Groven, S. Dutta, M. I. Popovici, N. Heylen, I. Ciofi, K. Vanstreels, F. W. Østerberg, O. Hansen, D. H. Petersen, K. Opsomer, C. Detavernie, C. J. Wilson, S. V. Elshocht, K. Croes, J. Bömmels, Z. Tőkei and C. Adelmann, *ACS Appl. Mater. Interfaces*, 2016, **8**, 26119–26125.
14 L. G. Wen, C. Adelmann, O. V. Pedreira, S. Dutta, M. Popovici, B. Briggs, N. Heylen, K. Vanstreels, C. J. Wilson, S. Van Elshocht, K. Croes, J. Bommels and Z. Tokei, in *2016 IEEE International Interconnect Technology Conference/Advanced Metallization Conference (IITC/AMC)*, IEEE, San Jose, CA, USA, 2016, pp. 34–36.
15 C. Adelmann, L. G. Wen, A. P. Peter, Y. K. Siew, K. Croes, J. Swerts, M. Popovici, K. Sankaran, G. Pourtois, S. Van Elshocht, J. Bommels and Z. Tokei, in *IEEE International Interconnect Technology Conference*, IEEE, San Jose, CA, USA, 2014, pp. 173–176.
16 M. H. Van Der Veen, A. Farokhnejad, A. K. Mandal, H. Struyf, S. Park and Z. Tőkei, in *2024 IEEE International Interconnect Technology Conference (IITC)*, IEEE, San Jose, CA, USA, 2024, pp. 1–3.
17 B. Hudec, K. Husekova, J. Aarik, A. Tarre, A. Kasikov and K. Frohlich, in *The Eighth International Conference on Advanced Semiconductor Devices and Microsystems*, IEEE, Smolenice, Slovakia, 2010, pp. 341–344.
18 K. Hušeková, E. Dobročka, A. Rosová, J. Šoltýs, A. Šatka, F. Fillot and K. Fröhlich, *Thin Solid Films*, 2010, **518**, 4701–4704.
19 Q. Li, S. Zheng, Y. Xu, H. Xue and H. Pang, *Chem. Eng. J.*, 2018, **333**, 505–518.
20 S. H. Choudhury, G. Vignaud, P. Dubreuil, B. D. Assresahegn, D. Guay and D. Pech, *Nanotechnology*, 2022, **33**, 495404.
21 Y. Qin, T. Yu, S. Deng, X.-Y. Zhou, D. Lin, Q. Zhang, Z. Jin, D. Zhang, Y.-B. He, H.-J. Qiu, L. He, F. Kang, K. Li and T.-Y. Zhang, *Nat. Commun.*, 2022, **13**, 3784.
22 X. Li, G. Chen, Y. Liu, R. Lu, C. Ma, Z. Wang, Y. Han and D. Wang, *Energy Environ. Sci.*, 2025, **18**, 4200–4209.
23 Z. Feng, X. Zhou, L. Šmejkal, L. Wu, Z. Zhu, H. Guo, R. González-Hernández, X. Wang, H. Yan, P. Qin, X. Zhang, H. Wu, H. Chen, Z. Meng, L. Liu, Z. Xia, J. Sinova, T. Jungwirth and Z. Liu, *Nat. Electron.*, 2022, **5**, 735–743.

24 S. M. Hussain and K. Son, *Phys. B*, 2025, **716**, 417723.
25 R. Gaur, L. Mishra, A. M. Siddiqi and B. Atakan, *RSC Adv.*, 2014, **4**, 33785–33805.
26 Y. Kotsugi, S.-M. Han, Y.-H. Kim, T. Cheon, D. K. Nandi, R. Ramesh, N.-K. Yu, K. Son, T. Tsugawa, S. Ohtake, R. Harada, Y.-B. Park, B. Shong and S.-H. Kim, *Chem. Mater.*, 2021, **33**, 5639–5651.
27 Y. Kim, M. Kim, Y. Kotsugi, T. Cheon, D. Mohapatra, Y. Jang, J. Bae, T. E. Hong, R. Ramesh, K. An and S. Kim, *Adv. Funct. Mater.*, 2022, **32**, 2206667.
28 H.-M. Kim, J.-H. Lee, S.-H. Lee, R. Harada, T. Shigetomi, S. Lee, T. Tsugawa, B. Shong and J.-S. Park, *Chem. Mater.*, 2021, **33**, 4353–4361.
29 D. Z. Austin, M. A. Jenkins, D. Allman, S. Hose, D. Price, C. L. Dezelah and J. F. Conley, *Chem. Mater.*, 2017, **29**, 1107–1115.
30 H. Wang, R. G. Gordon, R. Alvis and R. M. Ulfig, *Chem. Vap. Deposition*, 2009, 312–319.
31 H. Li, D. B. Farmer, R. G. Gordon, Y. Lin and J. Vlassak, *J. Electrochem. Soc.*, 2007, **154**, D642–D647.
32 M. Gock, M. Unkrig-Bau, J.-N. Huster, D. Zanders, J. Obenlüneschloß and A. Devi, *DE Pat*, WO2024223093A1, Heraeus Precious Metals GmbH & Co. KG, 2024.
33 R. G. Gordon, in *Atomic Layer Deposition for Semiconductors*, ed. C. S. Hwang, Springer US, Boston, MA, 2014, pp. 15–46.
34 A. V. Lee and L. L. Schafer, *Eur. J. Inorg. Chem.*, 2007, **2007**, 2245–2255.
35 M. D. Straub, S. Hohloch, S. G. Minasian and J. Arnold, *Dalton Trans.*, 2018, **47**, 1772–1776.
36 R. G. Gordon, H. Li, T. Aaltonen, B. S. Lim and Z. Li, *Open Inorg. Chem. J.*, 2008, **2**, 11–17.
37 H. Nakatsubo, D. Mohapatra, E. Lee, J. Kim, I. Cho, M. Iseki, T. Shigetomi, R. Harada, S. Na, T. Cheon, B. Shong and S. Kim, *Adv. Sci.*, 2025, e19209.
38 S.-S. Yim, D.-J. Lee, K.-S. Kim, S.-H. Kim, T.-S. Yoon and K.-B. Kim, *J. Appl. Phys.*, 2008, **103**, 113509.
39 A. Rothman, S. Seo, J. Woodruff, H. Kim and S. F. Bent, *J. Vac. Sci. Technol., A*, 2024, **42**, 052402.
40 M. D. Straub, J. Leduc, M. Frank, A. Raauf, T. D. Lohrey, S. G. Minasian, S. Mathur and J. Arnold, *Angew. Chem., Int. Ed.*, 2019, **58**, 5749–5753.
41 A. L. Catherall, M. S. Hill, A. L. Johnson, G. Kociok-Köhn and M. F. Mahon, *J. Mater. Chem. C*, 2016, **4**, 10731–10739.
42 M. D. Straub, E. T. Ouellette, M. A. Boreen, J. A. Branson, A. Ditter, A. L. D. Kilcoyne, T. D. Lohrey, M. A. Marcus, M. Paley, J. Ramirez, D. K. Shuh, S. G. Minasian and J. Arnold, *Chem. Commun.*, 2021, **57**, 4954–4957.
43 S. V. Ivanov, W. H. Bailey, X. Lei and D. P. Spence, US Pat, 8642797B2, *Air Products and Chemicals*, Inc., 2014.
44 P. S. Pregosin, *NMR in Organometallic Chemistry*, Wiley-VCH, Weinheim, Online-Ausg., 2012.
45 F. Neumann, H. Stoeckli-Evans and G. Süss-Fink, *J. Organomet. Chem.*, 1989, **379**, 139–150.
46 Q.-R. Xie, *Acta Crystallogr., Sect. E: Struct. Rep. Online*, 2008, **64**, o1110–o1110.
47 N. Boysen and A. Devi, *Eur. J. Mass Spectrom.*, 2023, **29**, 12–20.
48 D. M. Price, *Thermochim. Acta*, 2001, **367–368**, 253–262.
49 G. V. Kunte, S. A. Shivashankar and A. M. Umarji, *Meas. Sci. Technol.*, 2008, **19**, 025704.
50 K. Gregorczyk, L. Henn-Lecordier, J. Gatineau, C. Dussarrat and G. Rubloff, *Chem. Mater.*, 2011, **23**, 2650–2656.
51 S. Rushworth, R. Odedra, P. Viswanathan, S. Dosanjh and I. Lealman, *J. Cryst. Growth*, 2008, **310**, 4712–4714.
52 H. J. Jung, J. H. Han, E. A. Jung, B. K. Park, J.-H. Hwang, S. U. Son, C. G. Kim, T.-M. Chung and K.-S. An, *Chem. Mater.*, 2014, **26**, 7083–7090.
53 J. M. Hwang, S.-M. Han, H. Yang, S. Yeo, S.-H. Lee, C. W. Park, G. H. Kim, B. K. Park, Y. Byun, T. Eom and T.-M. Chung, *J. Mater. Chem. C*, 2018, **6**, 972–979.
54 G. Fang, L. Xu, Y. Cao and A. Li, *Coord. Chem. Rev.*, 2016, **322**, 94–103.
55 B. Van Der Linden, G. Pourtois, L. Nyns, S. Clima, T. Peissker and A. Delabie, *J. Phys. Chem. C*, 2025, **129**, 19573–19585.
56 F. Preischel, K. Rönnby, L. Mai, D. Zanders, D. Rogalla, B. Mallick, M. Nolan and A. Devi, *J. Am. Chem. Soc.*, 2025, **147**, 31764–31778.
57 (*a*) CCDC 2487934: Experimental Crystal Structure Determination, 2026, DOI: 10.5517/ccdc.csd.cc2phwy1; (*b*) CCDC 2487935: Experimental Crystal Structure Determination, 2026, DOI: 10.5517/ccdc.csd.cc2phwz2.